Journal of Power Sources 223 (2013) 221–231

Contents lists available at SciVerse ScienceDirect

Journal of Power Sources

journal homepage: www.elsevier.com/locate/jpowsour

Synthesis of Pt–Ir catalysts by coelectrodeposition: Application to ammonia electrooxidation in alkaline media

Steven Le Vot [a,b], Lionel Roué [a], Daniel Bélanger [b,*]

[a] INRS Energie, Matériaux et Télécommunications, 1650 bd. Lionel Boulet, Varennes, QC J3X 1S2, Canada
[b] Département de Chimie, Université du Québec à Montréal, CP 8888, Montréal, QC H3C 3P8, Canada

HIGHLIGHTS

- By changing deposition conditions, Ir fraction varies from 5 to 55 at. %.
- The activity for NH_3 oxidation depends on the electrode composition.
- Ir permits to lower the poisoning effect during NH_3 oxidation.
- For NH_3 concentrations lower than 0.02 M, Pt_{90}–Ir_{10} electrode show better activity.
- For low oxidation potential, the $Pt_{90}Ir_{10}$ electrode displays higher activity.

ARTICLE INFO

Article history:
Received 7 June 2012
Received in revised form
15 August 2012
Accepted 17 August 2012
Available online 21 September 2012

Keywords:
Pt–Ir
Electrochemical deposition
Ammonia oxidation
Electrocatalysis

ABSTRACT

The electrochemical activity for ammonia oxidation of $Pt_{(x)}$-$Ir_{(1-x)}$ electrodes prepared by coelectrodeposition on carbon substrate was investigated by cyclic voltammetry and potentiostatic methods. Morphologies of deposits were observed by field emission scanning electron microscopy and their chemical composition and crystallographic structure were analyzed by X-ray photoelectron spectroscopy and X-ray diffraction. It is demonstrated that the atomic composition of the catalysts is strongly influenced by the deposition conditions (e.g. relative concentration of the metallic complexes and deposition potential). Ammonia oxidation was investigated in alkaline media for concentrations varying from 0.005 to 0.1 M. Cyclic voltammetry experiments revealed an increase of activity for the $Pt_{(90)}$–$Ir_{(10)}$ electrode in comparison with Pt at low NH_3 concentration (<0.02 M). Moreover all the $Pt_{(x)}$–$Ir_{(1-x)}$ electrodes showed improved catalytic properties at low oxidation potentials (−0.55 to −0.4 V vs. Ag/AgCl) with respect to pure Pt. Finally, potentiostatic experiments indicated that an increase of the Ir content led to weaker poisoning effect of the resulting electrode despite that Ir does not seem to display a significant activity for the electrochemical oxidation of ammonia.

1. Introduction

Electrochemical oxidation of ammonia has recently attracted a lot of interest for both the viewpoint of wastewater treatment [1–6] and its possible application in direct ammonia fuel cell (DAFC) [7] and as a source of hydrogen which might be used in proton exchange membrane fuel cell (PEMFC) [8–11]. In this context, direct [12–14] and indirect [1–6] electrooxidation of NH_3 into N_2 have been widely studied in the past decade. The mechanism for NH_3 oxidation in alkaline media at a Pt electrode is a complex multi-step process [12–14]. It involves the successive dehydrogenation of nitrogen species and the formation of several adsorbed reaction intermediates on the electrode surface (Eqs. (1)–(6)) [15]:

$$NH_{3\ (aq)} \rightarrow NH_{3,\ ads} \quad (1)$$

$$NH_{3,\ ads} + OH^- \rightarrow NH_{2,\ ads} + H_2O + e^- \quad (2)$$

$$NH_{2,\ ads} + OH^- \rightarrow NH_{ads} + H_2O + e^- \quad (3)$$

$$NH_{x,\ ads} + NH_{y,\ ads} \rightarrow N_2H_{x+y,\ ads} \quad (4)$$

$$N_2H_{x+y,\ ads} + (x+y)\ OH^- \rightarrow N_2 + (x+y)\ H_2O + (x+y)\ e^- \quad (5)$$

* Corresponding author. Tel.: +1 514 987 3000x3909; fax: +1 514 987 4054.
E-mail address: belanger.daniel@uqam.ca (D. Bélanger).

0378-7753/$ – see front matter © 2012 Elsevier B.V. All rights reserved.
http://dx.doi.org/10.1016/j.jpowsour.2012.08.048

$$NH_{ads} + OH^- \rightarrow N_{ads} + H_2O + e^- \quad (6)$$

(with x=1 or 2 and y=1 or 2).

Pt electrode deactivates due to the formation of N_{ads} [15]. This intermediate acts as a poison because its high adsorption energy does not permit the recombination of two nitrogen adatoms and consequently no N_2 is formed [15]. The main findings concerning NH_3 oxidation on Pt electrode which are relevant for the understanding of this work can be summarized as follows. Differential electrochemical mass spectrometry (DEMS) measurements have shown that NH_3 is oxidized to N_2 at about −0.2 V vs. Ag/AgCl and to nitrogen oxides at potential more positive than −0.1 V due to the presence of a platinum oxides at the electrode surface [16]. At potential more positive than −0.1 V, the deactivation of Pt occurs because N_{ads} inactive intermediates are formed at the Pt surface [17]. Furthermore, the NH_3 oxidation is a structure sensitive reaction as it takes place almost exclusively on Pt(100) sites and that large Pt(100) terraces present the best electrocatalytic properties [18–22].

Because Pt deactivates, alternative anode materials have been studied for direct [12–14,17,23] and indirect [1–6] electrooxidation of NH_3 into N_2. For the direct electrochemical conversion of NH_3 to N_2, it appears that 5d noble transition metals (Pt and Ir) are the most active catalysts [17]. Lopez de Mishima et al. reported that the electrocatalytic activity of Pt_x–Ir_y (x=75, 50 and y=25, 50) alloys was higher than that of Pt and Ir black [24]. Despite that Pt–Ir electrodes seem to be very promising candidates for the NH_3 oxidation only a limited number of investigations have been reported in literature [7,8,24–29]. Endo et al. concluded that Ir plays a role in the dehydrogenation steps of ammonia (Eqs. (2), (3) and (6)) at low oxidation potential [25]. Interestingly, two recent studies reported that a Pt–Ir binary system inhibits Pt poisoning probably due to weak adsorption strength of N_{ads} intermediates [27,29]. In a study dealing with Pt–Ir electroplating on carbon fiber electrode, Pt–Ir were found to be good electrocatalysts for NH_3 electrolysis at low concentrations (20 mM) [26]. Moreover, alloying Ir and Pt permits to decrease the voltage of an ammonia electrolytic cell for the production of hydrogen [8].

Electrochemical deposition is a very attractive technique to prepare electrocatalysts due to its versatility, the high purity of the deposits and the possibility to readily control the loading of the deposits [30]. Moreover, electroplated nanoparticles usually exhibit better adhesion to the substrate with respect to chemical deposition [31]. On one hand, Pt electrodeposition has been widely studied in the literature [30,32–35]. On the other hand, Ir electrodeposition is a more complex process because it is strongly dependent of the substrate used and the deposition efficiency is very low [31,36–40]. To achieve iridium deposition on carbon, a large overpotential is required to form the first Ir nuclei on the surface [40]. Once these nuclei have been formed, hydrogen adsorption occurs on these sites and iridium deposition is catalyzed because H_{ads} acts as a reducing agent for Ir^{3+} [38,40]. This leads to the formation of large aggregates (several micrometers) of iridium but with very low faradaic efficiencies due to the occurrence of the competitive hydrogen evolution reaction. The surface density of such aggregates has been also found to be very low [40]. Contrariwise, on a platinum substrate, Ir deposition is fast because a high H_{ads} coverage is present at the electrode surface at much more positive potential than on carbon [40–43]. Moran et al. reported the preparation of $Pt_{70}Ir_{30}$ alloy using chloroplatinic acid and iridium chloride with an atomic ratio 1:1 [27]. Recently Boggs and Botte, investigated Pt–Ir coelectrodeposition on carbon fiber paper and conclude that atomic ratio, concentration of metal salts and applied potential directly influence the atomic composition of the synthesized electrodes and the plating efficiencies [28].

In this work, the electrochemical oxidation of ammonia on $Pt_{(x)}Ir_{(1-x)}$ ($45 < x < 100$) electrodeposited onto graphite and glassy carbon electrode was investigated. The purpose of this work is twofold. Firstly, it aims at investigating the influence of the deposition parameters on the morphology and the atomic composition of the $Pt_{(x)}$–$Ir_{(1-x)}$ electrodes. Secondly, the electrocatalytic properties of the electrodes were investigated in the presence of ammonia in alkaline media (1 M KOH). A wide range of $Pt_{(x)}$–$Ir_{(1-x)}$ electrodes, in terms of atomic compositions, were tested for several ammonia concentrations in order to get more insight in the role of Ir on the electrochemical activity of the Pt–Ir binary system for the ammonia oxidation.

2. Experimental

2.1. Electrode preparation

$Pt_{(x)}$–$Ir_{(1-x)}$ electrocatalysts were prepared by co-electrodeposition from hydrogen hexachloroplatinate (H_2PtCl_6) and iridium chloride ($IrCl_3$) (Aldrich, >99.9%) dissolved in a 0.5 M H_2SO_4 (Fisher, >95%) solution. Graphite (grade 2020, Test Solutions) and glassy carbon (diam. = 3 mm) electrodes (BASi) were used as substrates for the preparation of supported $Pt_{(x)}$–$Ir_{(1-x)}$ electrodes. All solutions were prepared using Nanopure water ($\rho > 18.0$ MΩ cm^{-1}) and degassed by bubbling with nitrogen (grade 4.8) for 30 min. Graphite plates (1.4 cm^2) were carefully polished and a three-step ultrasonic treatment (60 min in Nanopure water, 30 min in 1 M HNO_3 and 30 min in CH_3OH) was performed before each deposition to remove impurities. Glassy carbon electrodes were also carefully polished but the ultrasonic treatment lasted only for 5 min in Nanopure water. The electrodeposition was performed either by cyclic voltammetry or at constant potential. Graphite and glassy carbon electrodes were immersed in the deposition solution at a potential at which spontaneous deposition of Pt and Ir is negligible (around 0.6 V vs Ag/AgCl). The potential was then scanned between 0.6 and −0.2 V vs Ag/AgCl for cyclic voltammetry experiments or shifted to the desired value for potentiostatic deposition. The aim is to obtain deposits with different $Pt_{(x)}$–$Ir_{(1-x)}$ atomic compositions and to compare their influence on the NH_3 electrooxidation.

2.2. Electrochemical measurements

Electrochemical characterizations were carried out at room temperature in a typical one-compartment cell using a three-electrode configuration with a potentiostat/galvanostat VMP3 (BioLogic Science Instrument). An Ag/AgCl reference electrode ($E^0 = 0.199$ V vs. NHE) and a platinum gauze counter electrode were used for all experiments performed in acid media. In alkaline media, a Hg/HgO (1 M KOH) was used as reference electrode. The H_{ads} coverage and the electroactive surface area of the Pt and $Pt_{(x)}$–$Ir_{(1-x)}$ deposits were estimated from the voltammetric charge associated with the adsorption of hydrogen (between 0.2 and −0.2 V Vs. Ag/AgCl in a 0.5 M H_2SO_4 aqueous solution; scan rate = 50 mV s^{-1}). The electroactive surface area (S) of Pt and Pt–Ir electrodes were estimated by using the conversion factor of 210 μC cm^2 [44,45] corresponding to the charge for the reduction of a monolayer of adsorbed hydrogen assuming that one hydrogen is adsorbed on each Pt site exposed to the electrolyte (data not shown) [38,40,44,46–48]. The electrocatalytic activity of the $Pt_{(x)}$–$Ir_{(1-x)}$ electrodes for NH_3 oxidation were investigated by cyclic voltammetry and potentiostatic experiments in 1 M KOH + x M NH_3 ($0.005 < x < 0.1$).

2.3. Sample characterization

X-ray photoelectron spectroscopy (XPS) spectra were collected on AXIS ULTRA spectrometer (Kratos Analytical) at the Alberta Centre for Surface Engineering and Science (ACSES), University of

Alberta. The base pressure in the analytical chamber was lower than 2×10^{-8} Pa. Monochromatic Al K_α source ($h\nu = 1486.6$ eV) was used at a power of 210 W. The analysis spot was 700 × 400 μm. Survey scans were collected for binding energy from 1100 to 0 eV with analyzer pass energy of 160 eV and a step of 0.35 eV. For the quantification of $Pt_{(x)}$–$Ir_{(1-x)}$ atomic composition, Ir 4f (60–70 eV) et Pt 4f (70–80 eV) peaks were used. The X-ray diffraction (XRD) spectra were collected with a Bruker AXSD8 Siemens X-ray diffractometer operating with a CuK_α radiation ($\lambda = 0.154$ nm) generated at 40 kV and 40 mA. A small-angle (2°) θ–2θ scan mode was used with an angular step size of $2\theta = 0.02°$ and an acquisition of 5 s by step. Morphologies of $Pt_{(x)}$–$Ir_{(1-x)}$ deposits on carbon were observed by field emission scanning electron microscopy (FE-SEM) using a JEOL JSM − 7600 TFE microscope at an accelerating voltage of 5 kV.

For experimental purposes, graphite substrates were used for physicochemical characterization whereas glassy carbon electrodes were preferred for electrochemistry measurements. However, it is important to point out that both substrates were tested for all experiments of this study and that in our experimental conditions both types of carbon substrates gave similar results.

3. Results and discussion

3.1. Cyclic voltammetry of carbon in the presence of platinum and iridium salt in the solution

Fig. 1 shows the cyclic voltammograms (CVs) for the first and 40th scans for glassy carbon electrodes in 0.5 M H_2SO_4 in the presence of 1 mM $PtCl_6^{2-}$, 3 mM Ir^{3+} and a mixture of 1 mM H_2PtCl_6 and 3 mM $IrCl_3$. In all cases the potential is scanned from 0.6 V, which corresponds to a potential at which Ir or Pt is not deposited because spontaneous deposition can be considered as negligible due to its very slow rate [31,32,49], to a potential of −0.2 V, just prior to the onset of the hydrogen evolution reaction (HER) on Pt and Ir [38,44]. Firstly, in the presence of Ir^{3+} ions (Fig. 1a), only capacitive current is observed and the shape of CV does not change with cycling during 40 cycles indicating that iridium is not deposited on the carbon surface. This is in good agreement with our previous study in which it was demonstrated that a very negative potential, of at least −0.6 V, must be reached to achieve iridium deposition on glassy carbon [40]. Secondly, in the presence of $PtCl_6^{2-}$ ions (Fig. 1b), the onset of the cathodic current noticed at 0.45 V is followed by a broad cathodic current wave at 0.1 V and a well-defined peak at −0.1 V, attributed to the electrodeposition of Pt [50]. Finally, in the presence of 3 mM Ir^{3+}+1 mM $PtCl_6^{2-}$ ions (Fig. 1c), the onset of the cathodic current is noticed at 0.3 V and a low intensity peak is observed at −0.12 V just before an abrupt increase of the cathodic current. Following scan reversal, the observation of a nucleation loop is consistent with metal deposition on the glassy carbon electrode surface and an increase of the electrode surface area [51]. Moreover, a cathodic current is always observed between 0.6 and −0.2 V indicating that, presumably, the reduction of metal complexes is still occurring. On Fig. 1b, the CV for the 40th cycle (dashed line), in the presence of only $PtCl_6^{2-}$ ions in the solution, is very similar to that of a platinum electrode in sulfuric acid which is characterized by its so-called hydrogen adsorption region between 0.2 and −0.2 V [32,40,43,44]. Since iridium alone cannot be deposited between 0.6 and −0.2 V whereas Pt can, one could expect that in the presence of Ir^{3+} and $PtCl_6^{2-}$ ions in the solution, only platinum could be deposited on glassy carbon. However, the shape of the 40th cycle (Fig. 1c) differs significantly from that expected for a Pt electrode and is more like the one observed for Ir or Pt–Ir electrodes [52,53]. In this work, the morphology and composition of Pt–Ir deposits were characterized by SEM, XRD and XPS.

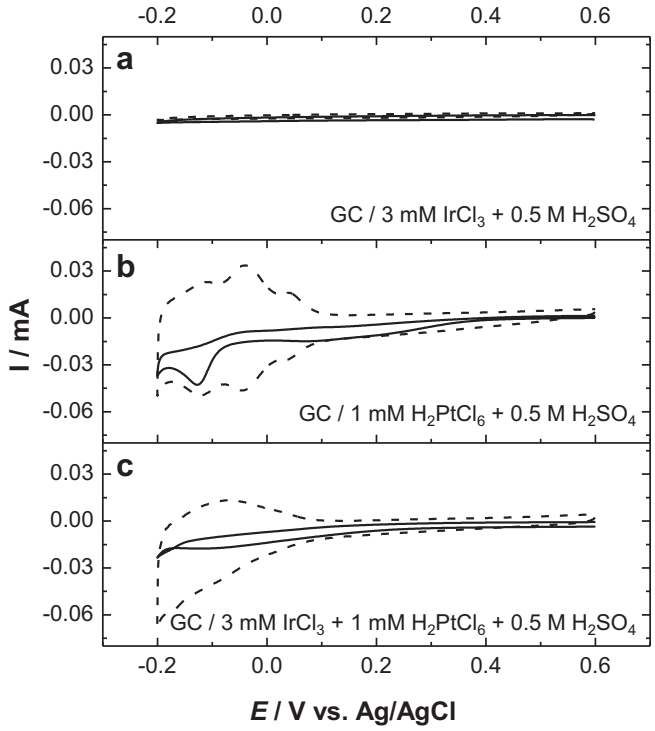

Fig. 1. Cyclic voltammogram of glassy carbon electrodes in the presence of: a) 3 mM $IrCl_3$ + 0.5 M H_2SO_4; b) 1 mM H_2PtCl_6 + 0.5 M H_2SO_4 and c) 3 mM $IrCl_3$ + 1 mM H_2PtCl_6 + 0.5 M H_2SO_4 at a scan rate of 50 mV s^{-1}. First (black), and 40th (dashed black) cycles.

3.2. Morphologies of the Pt–Ir deposits observed by SEM

Morphologies of $Pt_{(x)}$–$Ir_{(1-x)}$ deposits on graphite electrodes were observed by field emission scanning electron microscopy. Fig. 2 compares a set of nine electrodes for which the deposition potential and the $[Ir^{3+}]/[PtCl_6^{2-}]$ ratio in the deposition solution were varied. When the deposition potential is set to 0 and −0.1 V, the deposits looks like spherical aggregates whereas for a deposition potential of −0.2 V, the surface consists of aggregates covered by platinum needles. Interestingly, this trend is the same than for platinum deposition alone [30,54]. Moreover, it seems that the surface coverage is more important for deposition at −0.1 and −0.2 V than at 0 V. On the other hand, morphologies of deposits seem not to be affected by the $[Ir^{3+}]/[PtCl_6^{2-}]$ ratio but the sizes of $Pt_{(x)}$–$Ir_{(1-x)}$ aggregates appear to be a little smaller when this ratio is increased. Fig. 3 shows the size distribution of $Pt_{(x)}$–$Ir_{(1-x)}$ aggregates for coatings deposited in various conditions by taking into account 600 aggregates in each case. Increasing the $[Ir^{3+}]/[PtCl_6^{2-}]$ ratio leads to a slight decrease of aggregates size. Moreover, it can be noticed that a high $[Ir^{3+}]/[PtCl_6^{2-}]$ ratio yields more homogeneous aggregate sizes. On the other hand, the deposition potential has no effect on $Pt_{(x)}$–$Ir_{(1-x)}$ aggregate sizes.

3.3. XRD characterization of $Pt_{(x)}$–$Ir_{(1-x)}$ electrodes

A set of eleven electrodes were prepared by using the conditions given in Table 1 and characterized by X-ray diffraction. Fig. 4 shows XRD patterns of $Pt_{(x)}$–$Ir_{(1-xx)}$ electrodeposits and focuses on the characteristic (111) peak. A shift of the (111) peak to higher 2Θ values relative to a pure Pt layer is observed for deposits obtained when Ir was present in the deposition solution. From the 2Θ values, the atomic composition of the electrodes was estimated by using Vegard's law [27]. The Pt at. % of each deposit is also indicated in

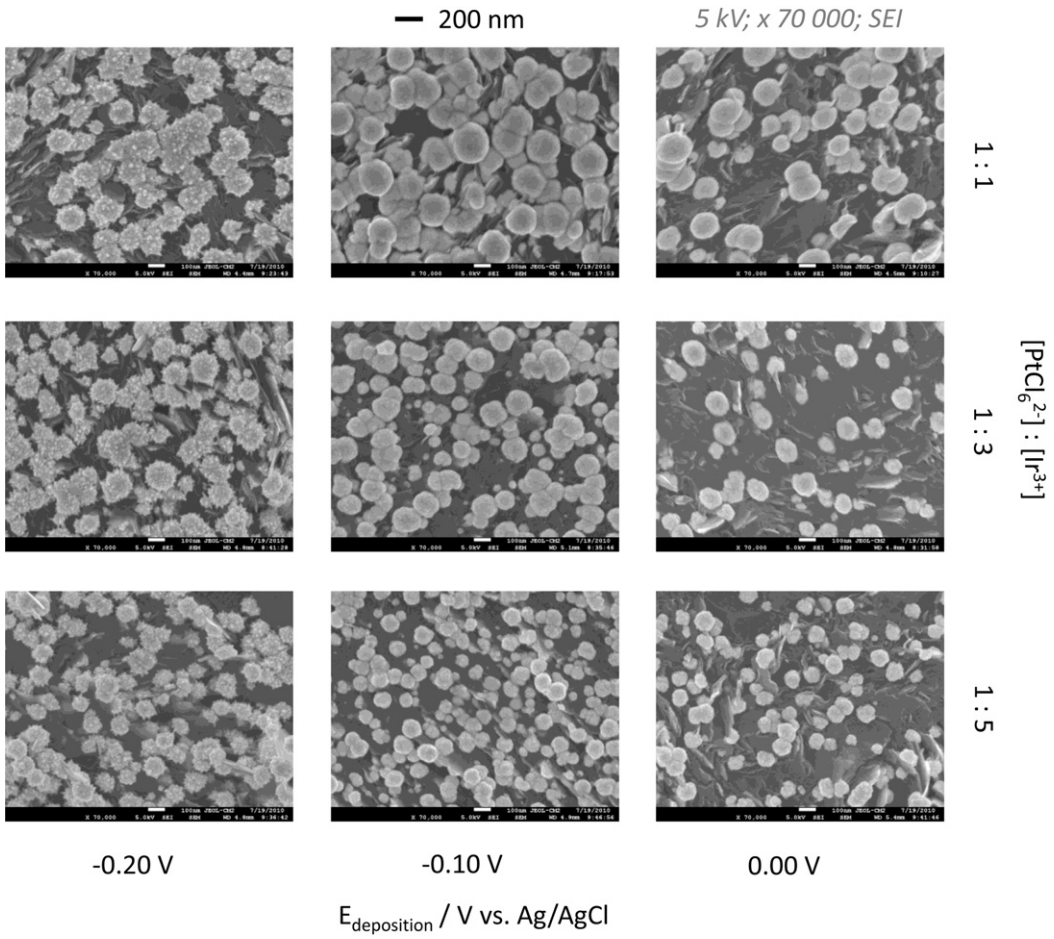

Fig. 2. FESEM images of $Pt_{(x)}$–$Ir_{(1-x)}$ electrodes prepared by electrodeposition as a function of $[PtCl_6^{2-}]/[Ir^{3+}]$ ratio and deposition potential.

Fig. 4. The XRD data show that the deposits are always much richer in Pt than in the deposition bath. Actually, in our experimental conditions, it was not possible to deposit a film with an Ir fraction larger than 50 at. %. Even with a Ir/Pt ratio of 5 in the deposition bath, the Ir fraction is only 48 at. %. Finally the optimum potential to obtain the highest loading of Ir is about −0.1 V (see below). At −0.2 V, Pt deposition is highly favored leading to a Pt fraction of about 90 at. %. In our experimental conditions, Ir cannot be deposited alone on a carbon substrate, explaining why a pattern for 100 at. % Ir is not presented on Fig. 4 [40]. It can be noticed that not only the 2Θ value but also the full width at half maximum (FWHM) of the (111) peak change with the atomic composition of the electrodes. The average crystallite size of $Pt_{(x)}$–$Ir_{(1-x)}$ electrodeposits was estimated using Scherrer equation. It can be seen that the size of the crystallites decreases (from 15 to 5 nm) when the Ir fraction in the deposit is increasing [55,56].

3.4. XPS characterization of $Pt_{(x)}$–$Ir_{(1-x)}$ electrodes

In order to determine the surface atomic composition of the $Pt_{(x)}$–$Ir_{(1-x)}$ electrodes, XPS analyses were carried out to complement the XRD data. Fig. 5 shows survey spectra recorded for graphite electrodes that are characterized by the presence of Pt 4f (between 70 and 80 eV) and Ir 4f (60 and 70 eV) contributions [38,40,57]. The Pt $4f_{7/2}$ peak observed at around 71.8–72 eV is in relatively good agreement with the binding energy expected for metallic Pt (71.6 eV) [58–60]. The survey spectrum (between 60 and 70 eV) for a pure Ir deposit (#10 on Fig. 5) indicates the presence of at least three different species. Indeed, in our experimental conditions, the presence of metallic Ir, IrO_2 and the $IrCl_3$ precursor is demonstrated [38,40,61]. The presence of the latter is confirmed by the Cl 2p peak (200 eV) on the survey spectra (data not shown). For the Pt–Ir electrodes the Ir 4f contribution (between 60 and 70 eV) corresponds to metallic Ir [38,40,55,56]. The atomic composition of the surface of the electrodes was determined from these survey spectra and included on Fig. 5. It can be noticed that Pt atomic composition varies from about 50 to 90 at. % which appears to be in qualitative agreement with the composition derived from XRD measurements.

To get more insight into the Pt–Ir electrodeposition process, the influence of the deposition potential on the atomic composition of the Pt–Ir electrodes, prepared with a $[Ir^{3+}]/[PtCl_6^{2-}]$ ratio of 3:1 was investigated. Fig. 6 shows the evolution of Pt content (Pt at. %) determined by XPS measurements of the electrodes as a function of the deposition potential. A minimum of Pt at. % and thus a maximum Ir content is observed for a deposition potential of around −0.07 V. It is very interesting to notice that the trend described in Fig. 6 for Pt–Ir co-electrodeposition is in perfect agreement with conclusions of a previous study dealing with Ir deposition on platinum [40]. Considering the potential range used (0 to −0.2 V), it is very likely that the deposition mechanism of Pt–Ir on carbon substrate consists in a first step in which Pt is deposited on the surface (at such deposition potential Ir alone cannot be deposited onto a carbon surface [40]). As soon as Pt is deposited, H_{ads} occurs on these sites and catalyzes Ir deposition leading to the formation of a $Pt_{(x)}$–$Ir_{(1-x)}$ binary deposit. Fig. 6 also indicates that, under our experimental

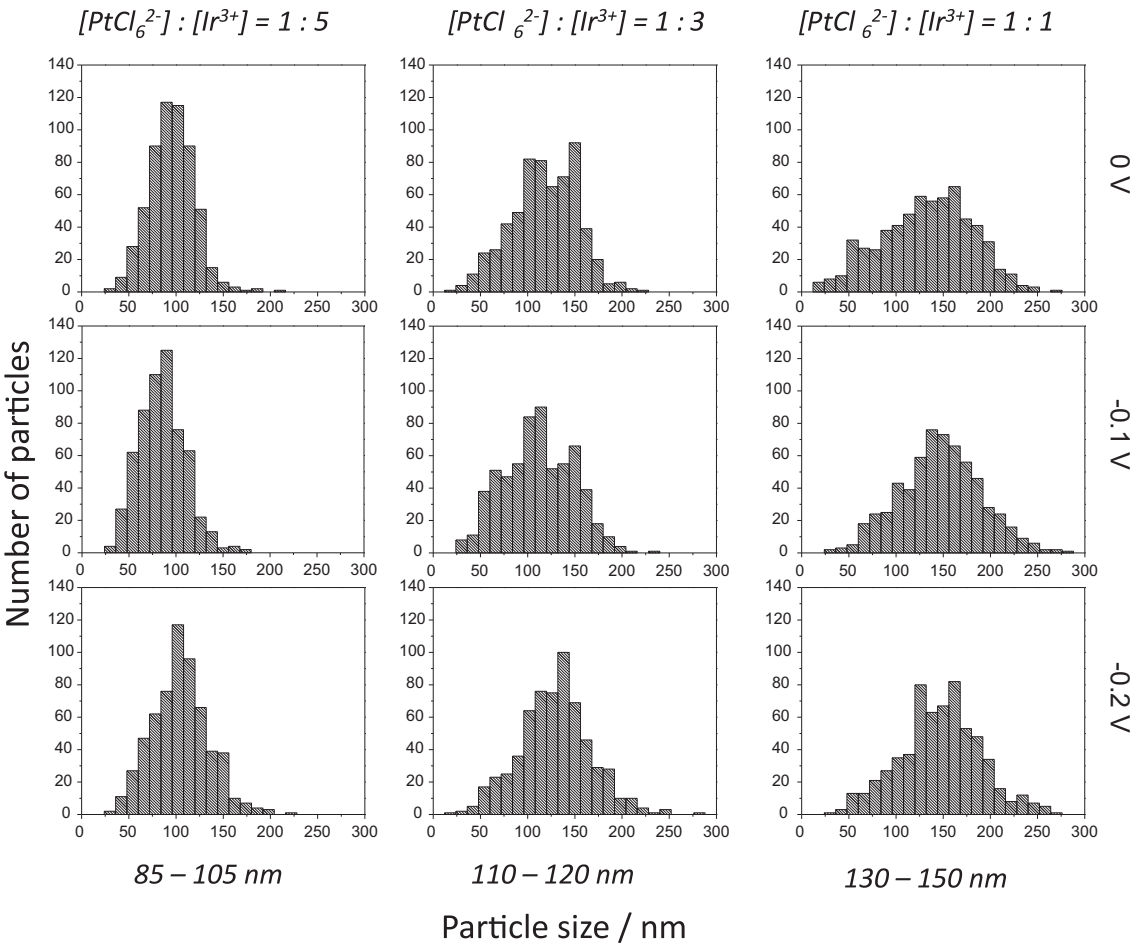

Fig. 3. Particle size distribution for $Pt_{(x)}$–$Ir_{(1-x)}$ electrodes prepared by electrodeposition as a function of $[PtCl_6^{2-}]/[Ir^{3+}]$ ratio and deposition potential.

conditions, electrochemical deposition does not allow to synthesize electrodes with Pt at. % smaller than 45%.

Fig. 7 shows a plot of the Pt at. % of $Pt_{(x)}$–$Ir_{(1-x)}$ electrodes estimated from XPS data as a function of their lattice parameter determined from XRD data. A linear relationship between these two parameters is observed, strongly suggesting that the variation of lattice parameters in the $Pt_{(x)}$–$Ir_{(1-x)}$ systems obey Vegard's law and thus that prepared $Pt_{(x)}$–$Ir_{(1-x)}$ catalysts are alloyed as a solid solution phase [55,62]. Moreover Fig. 7 and Table 1 indicate that the bulk (XRD) and the surface (XPS) compositions of the electrode are very close and thus that deposits are very homogeneous. For the remainder of the work which focuses on the electrochemical characterization of Pt–Ir electrodes for NH_3 oxidation, a deposition bath with a $[Ir^{3+}]/[PtCl_6^{2-}]$ ratio of 3 was used to prepare the various Pt–Ir electrodes.

Table 1
Experimental conditions used for the electrodeposition of Pt, Ir and $Pt_{(x)}$–$Ir_{(1-x)}$ electrodes and composition (Pt at. %) of the deposits as determined from XRD and XPS measurements.

Electrode	$[H_2PtCl_6]$ (mM)	$[IrCl_3]$ (mM)	*E* deposition (V)	XRD	XPS
1	1	1	0	60	63
2	1	1	−0.1	60	62
3	1	1	−0.2	87	95
4	1	3	0	58	55
5	1	3	−0.1	54	49
6	1	3	−0.2	89	94
7	1	5	0	60	56
8	1	5	−0.1	52	50
9	1	5	−0.2	90	92
10	0	1	−0.2	–	0
11	1	0	−0.2	100	100

3.5. Cyclic voltammetry of $Pt_{(x)}$–$Ir_{(1-x)}$ electrodes in the presence of NH_3

The cyclic voltammetry behavior of $Pt_{(x)}$–$Ir_{(1-x)}$ electrodes in 0.1 M NH_3 + 1 M KOH are compared in Fig. 8a. The CVs show a typical broad irreversible anodic peak at −0.25 V corresponding to NH_3 oxidation [12–14]. The maximum current is recorded for a pure Pt electrode and the intensity of the current peak decreases when the Pt content is lowered. A quantitative representation is depicted in Fig. 8b, which presents the evolution of the current density of the oxidation peak as a function of the Pt content of the electrodes. It should be noted that the current densities take into account the electroactive surface area determined form the H_{ads} region which probes the presence of both Pt and Ir [44,46–48]. Fig. 8b (square) shows that the ammonia oxidation peak current density is strongly affected by the composition of the Pt–Ir electrodes. A small current is recorded up to a Pt at. % of 60 and thereafter the electrochemical activity increases exponentially with the platinum content of the electrodes. The data of Fig. 8a was analyzed further by assuming that only Pt atoms are active for the electrochemical oxidation of ammonia. Thus, the current densities were normalized to the surface area of the Pt atoms of the deposits and are shown on Fig. 8b (triangle) as a function of the Pt at. %. If the normalized current of Fig. 8b would be only related to the surface

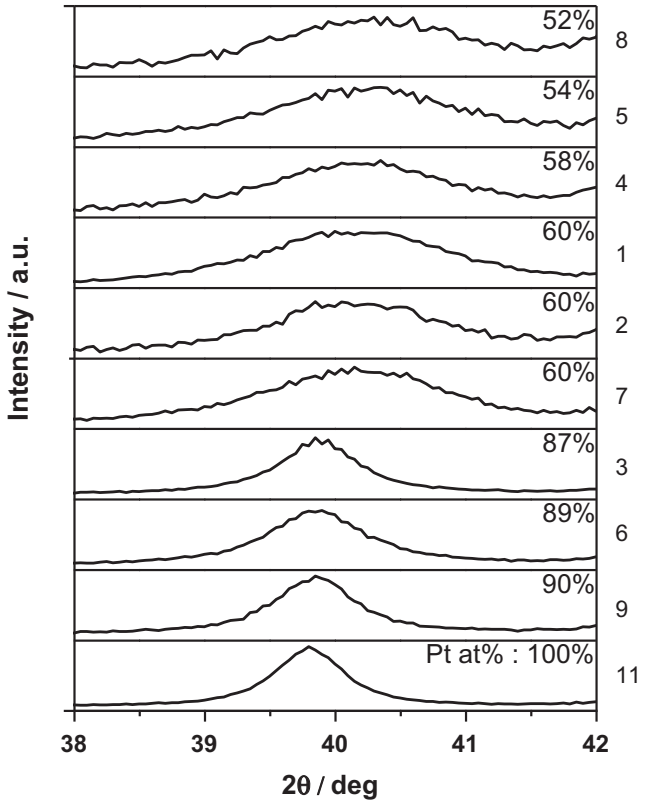

Fig. 4. X-ray diffractogram ((111) domain peak) of Pt and $Pt_{(x)}$–$Ir_{(1-x)}$ electrodes (see Table 1 for experimental conditions).

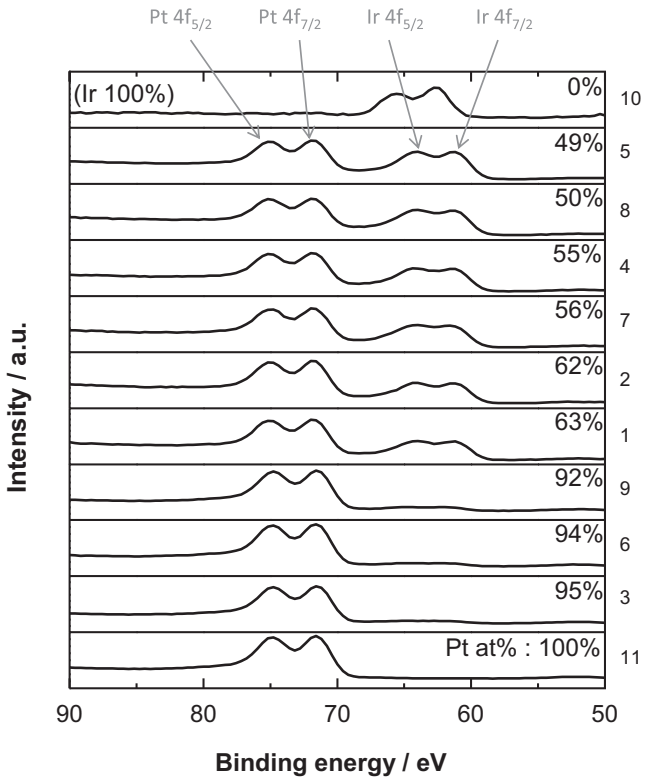

Fig. 5. X-ray photoelectron survey spectra for the Pt 4f (between 70 and 80 eV) and Ir 4f (between 60 and 70 eV) regions of Pt, Ir, and $Pt_{(x)}$–$Ir_{(1-x)}$ electrodes (see Table 1 for experimental conditions).

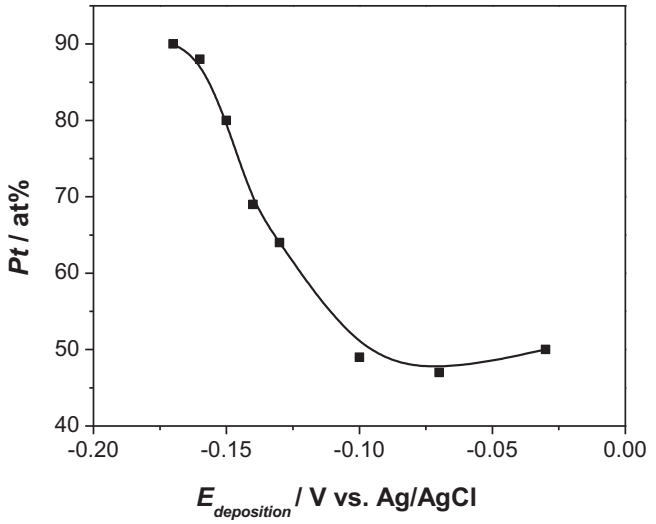

Fig. 6. Plot of the Pt at. % of the $Pt_{(x)}$–$Ir_{(1-x)}$ deposits prepared from a 1 mM H_2PtCl_6 + 3 mM $IrCl_3$ + 0.5 M H_2SO_4 during 60 min vs. the deposition potential.

area of Pt, a constant normalized peak current would be expected. In fact Fig. 8b shows clearly that this is not the case and that the addition of Ir to a Pt-based electrode decreases its activity for ammonia oxidation. The best activity was found for a pure Pt electrode leading to the conclusion that alloying Pt and Ir does not improve the electrocatalytic properties for ammonia oxidation with respect to pure Pt electrode. This is in agreement with Vidal-Iglesias et al. who demonstrated that Pt nanoparticles deposited on a Au substrate were better catalysts than binary nanoparticles (e.g., Pt–Ir) for ammonia oxidation in 0.2 M NaOH and 0.1 M NH_3 [7]. An heterogeneous distribution of Pt and Ir at the electrode surface and that distinct Pt and Ir regions could coexist was invoked to explain the decrease of electrochemical activity upon addition of Ir. Moreover, Ir not only replaces Pt atoms at the surface and thus contributes to a decrease of Pt electroactive area but Ir also decreases the density of Pt(100) sites and perturbs the long range order of the Pt(100) terraces that are the most active for ammonia electrooxidation [7,21,63].

Nonetheless, $Pt_{(x)}$–$Ir_{(1-x)}$ catalysts show interesting properties that could encourage to consider their use as alternatives to Pt

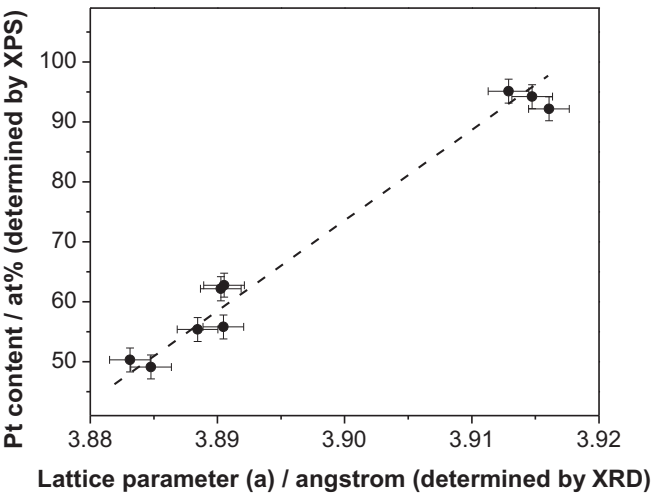

Fig. 7. Plot of the Pt at. % of the $Pt_{(x)}$–$Ir_{(1-x)}$ deposits (determined by XPS, Fig. 5) vs. the lattice constant of electrodes (determined by the diffraction angle of the (111) domain peaks, Fig. 4).

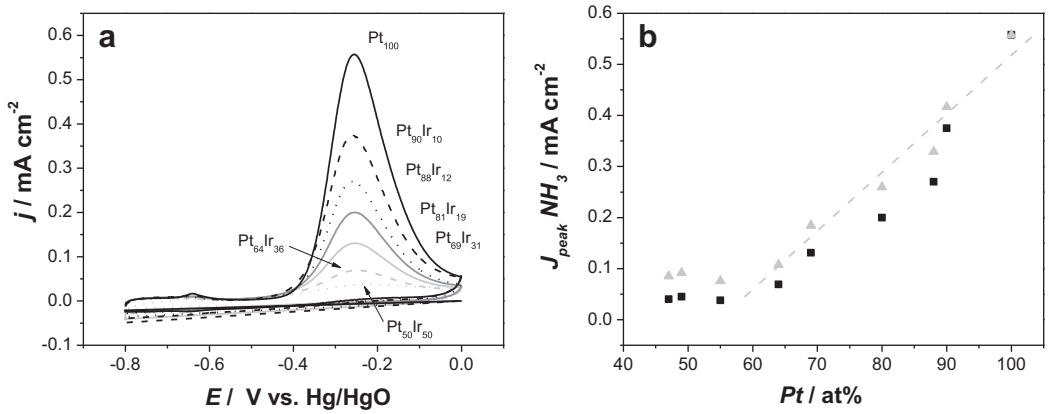

Fig. 8. a) Cyclic voltammograms of $Pt_{(x)}$–$Ir_{(1-x)}$ electrodes in 0.1 M NH_3 + 1 M KOH. Scan rate = 20 mV s^{-1}. b) Current of the NH_3 oxidation peak as a function of Pt at. %. The current is normalized by considering the electrochemical active surface area of Pt and Ir (black square) and only the contribution of Pt surface atoms (grey triangle).

electrode. Firstly, the onset of NH_3 oxidation occurring at −0.52 V on platinum is slightly shifted toward more negative potentials when the Ir content increases. Secondly, the potential of the peak corresponding to the NH_3 oxidation observed at −0.26 V on pure Pt is slightly shifted toward more positive potential by up to 30 mV for $Pt_{50}Ir_{50}$. Thus, the slight shift of NH_3 oxidation peak potential to more positive potential when Ir is added could indicate that the addition of Ir inhibits platinum poisoning [17].

In order to further investigate this hypothesis, short (10 min) oxidation of NH_3 were performed at −0.25 V. Fig. 9 shows current-time responses for 3 selected electrodes. The electrocatalytic properties of a Pt catalyst used as a reference sample and two $Pt_{(x)}$–$Ir_{(1-x)}$ electrodes (one with high Ir content and the other one with low Ir content) are compared. As expected, the activity decreases when the Pt content is lowered. However, it is well-known that Pt electrodes deactivate with time during NH_3 electrolysis because adsorbed N-species formed by oxidation of ammonia poison the electrode [15–17,54]. The slope of I–t transients (for electrolysis time larger than about 100 s) were determined and values of -1.2×10^{-4}, -7.1×10^{-5} and -1.6×10^{-5} mA cm^{-2} s^{-1} were found for Pt, $Pt_{90}Ir_{10}$ and $Pt_{55}Ir_{45}$ electrodes, respectively. Interestingly, the current decreases twice faster for Pt than for $Pt_{90}Ir_{10}$ and seven times faster than for $Pt_{55}Ir_{45}$. This suggests that Ir alloyed to Pt inhibits the poisoning effect of the electrodes during ammonia electrolysis [54].

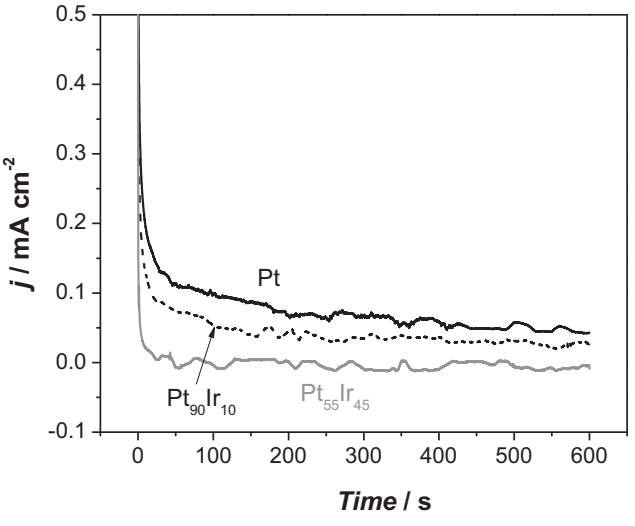

Fig. 9. Current–time response for Pt (black), $Pt_{90}Ir_{10}$ (dash) and $Pt_{55}Ir_{45}$ (grey) electrodes in 0.1 M NH_3 + 1 M KOH for an applied potential of −0.25 V.

3.6. Effect of NH_3 concentration on cyclic voltammetry of $Pt_{(x)}$–$Ir_{(1-x)}$ electrode

In order to get more insight in the exact role of iridium on the electrochemical activity of $Pt_{(x)}$–$Ir_{(1-x)}$ electrodes, the effect of NH_3 concentration was investigated. Fig. 10 shows the cyclic voltammograms for Pt and Pt_{90}–Ir_{10} electrodes for 5 different NH_3 concentrations ranging between 0.005 and 0.08 M. In all cases, the onset of NH_3 oxidation occurs at potential more negative for the Pt_{90}–Ir_{10} electrode (i.e., at −0.54 V compared to −0.49 V on Pt). Moreover, it can be noticed that for low oxidation potentials (from −0.55 to −0.40 V) the Pt_{90}–Ir_{10} electrode exhibits better activity than pure Pt. Fig. 10 also shows that the intensity of the anodic peak current is higher for the Pt–Ir electrode when the ammonia concentration is lower than 0.02 M, whereas Pt is more active for more concentrated NH_3 solution. This is also illustrated in Fig. 11a which presents the plot of the current of the NH_3 oxidation peak as a function of the ammonia concentration for Pt and $Pt_{90}Ir_{10}$ electrodes. Furthermore, Fig. 11b clearly shows that the potential of this anodic peak is shifted toward more positive values for Pt_{90}–Ir_{10} indicating that Pt deactivates faster than the Pt–Ir electrode.

3.7. Cyclic voltammetry study of Pt and $Pt_{90}Ir_{10}$ electrodes poisoning

The aim of the following experiments is to try to understand why Pt–Ir is more efficient than Pt for low oxidation potential (−0.4 to −0.55 V) and low NH_3 concentration (<0.02 M). The key step of ammonia oxidation (rate determining step) is the recombination of two dehydrogenated NH_x intermediates [13,21]. Since the nature of intermediates strongly depends of the composition of the electrode and its potential [7,16–18,21], it is postulated that gradually varying the upper potential limit (from −0.55 to 0 V) of the CV scan and comparing Pt and $Pt_{90}Ir_{10}$ electrodes could provide interesting information about role played by Ir during ammonia oxidation.

Fig. 12 shows cyclic voltammograms for Pt and $Pt_{90}Ir_{10}$ electrodes for a high (0.08 M) and a low (0.005 M) NH_3 concentration. The first CV was performed from −0.8 to −0.55 V and the following ones were recorded by progressively increasing the positive potential limit with an increment of 50 mV until it reaches a value of 0 V. Before each CV, a potential of −0.8 V was applied during 20 s in order to reactivate the electrode [16,54]. For low NH_3 concentration (Fig. 12a and c) four anodic peaks corresponding to different

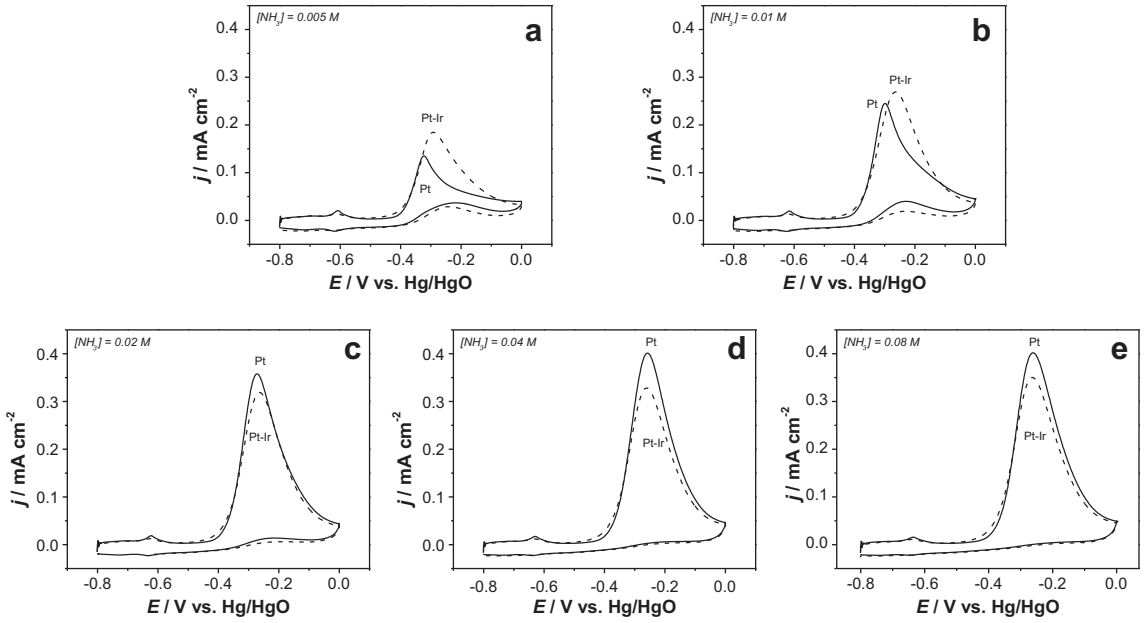

Fig. 10. Cyclic voltammograms of Pt (solid) and $Pt_{90}Ir_{10}$ (dashed) electrodes in 1 M KOH + *x* M NH_3. *x* = a) 0.005, b) 0.01, c) 0.02, d) 0.04 and e) 0.08. Scan rate = 20 mV s^{-1}.

steps of the complex mechanism of ammonia electrooxidation (Eqs. (1)–(6)) are observed [13,15,16,21]. Peaks A_1 and A_2 are attributed to ammonia dehydrogenation whereas peaks A_3 and A_4 correspond to the oxidation of adsorbed intermediates [21]. These intermediates could be reduced back to ammonia at around −0.6 V (peak C_1) [16]. Rosca and Koper further investigated peaks A_2/C_1 and associated them to a NH_2/NH_3 "reversible" reaction [21].

In our experiment, peaks A_2/C_1 are affected as the upper limit potential is increased. For Pt electrode (Fig. 12a), when the upper limit potential is more negative than −0.25 V (bolded line), the intensity of peaks A_2/C_1 and the voltammetric charge are independent of the CV potential limit. A very similar trend is observed with a Pt_{90}–Ir_{10} electrode (Fig. 12c). On the other hand, when the upper potential limit is shifted towards more positive potential than −0.25 V, the shape of CVs during the negative going scan is strongly affected between −0.4 and −0.8 V. Firstly, a significant cathodic current appears between −0.4 and −0.55 V even if the current of the scan in the positive direction is constant. Presumably, this current is due to a faradaic reaction corresponding to the reduction of adsorbed N-species. Secondly, the cathodic peak C_1 at −0.62 V is flattened when the positive potential limit is increased. This effect seems to be more pronounced for the $Pt_{90}Ir_{10}$ electrode in comparison to pure Pt. This could be an indication that the nature of adsorbed N-species changed when the positive potential limit it increased and that for potential more positive than −0.25 V, the electrode is mainly covered by NH_{ads} and N_{ads} which are inactive intermediates for nitrogen formation [17,21]. Moreover, a small peak C_2 appears at −0.72 V, whose intensity increases when the positive potential limit is increased. However, the corresponding peak A_1 in the anodic region does not evolve (or at least, only a very slight decrease can be observed) indicating that A_1 and C_2 are not related. Thus C_2 might be attributed to the desorption of the most strongly adsorbed intermediates (probably N_{ads}).

When the ammonia concentration is increased to 0.08 M (Fig. 12b and d), two noticeable differences are observed in the CVs. Firstly, the intensity of the NH_3 oxidation peak at −0.25 V is increased and secondly, the anodic peak A_4 (Fig. 12a and c) is not observed. This latter fact indicates that in the more concentrated NH_3 solution the electrode is more passivated. When the NH_3 concentration is increased, more reaction intermediates might be

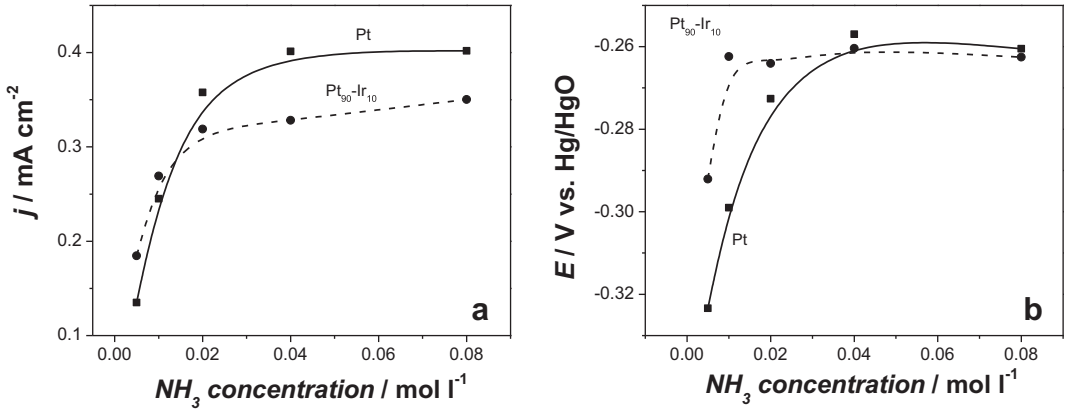

Fig. 11. Plot of the a) current density of the NH_3 oxidation peak b) potential of the NH_3 oxidation peak, as a function of NH_3 concentration for Pt and $Pt_{90}Ir_{10}$ electrodes.

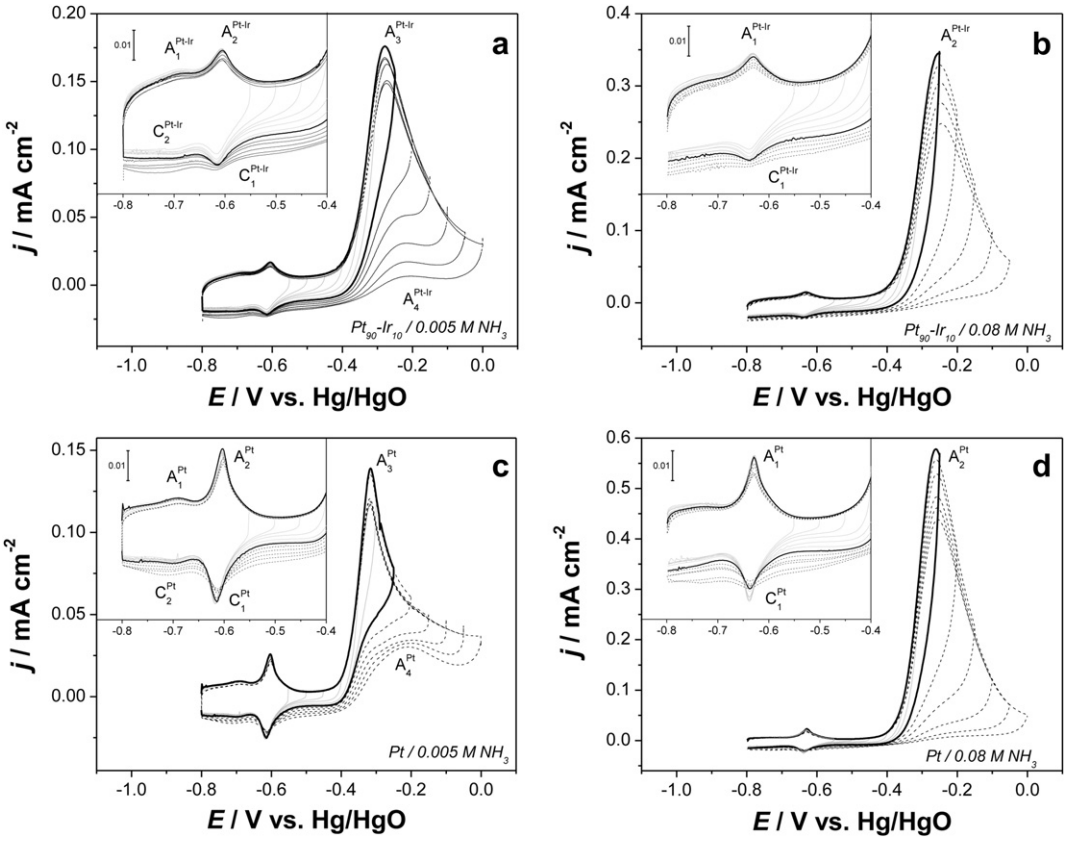

Fig. 12. Cyclic voltammograms of Pt_{90}–Ir_{10} and Pt electrodes in a) and c) 0.005 M NH_3 + 1 M KOH and b) and d) 0.08 M NH_3 + 1 M KOH. Upper potential limit was shifted from −0.55 to 0 V with an increment step of 0.05 V. Before each cyclic voltammogram (2nd cycle shown), a regeneration procedure was performed by applying a cathodic potential of −0.8 V during 20 s.

adsorbed, thus favoring the electrode poisoning effect. Further investigations are needed to determine the nature of these adsorbates and to get a better understanding of this phenomenon.

In order to get more insight into the NH_3 oxidation mechanism on Pt–Ir (and Pt), the evolution of the cyclic voltammograms between −0.4 and −0.8 V and the redox waves centered at −0.62 V were investigated. These redox waves correspond to the reversible NH_3/NH_2 redox couple [21]. Coulometric charges of both the anodic (Qa) and the cathodic (Qc) peaks were determined and their ratios are reported in Fig. 13 as a function of the positive potential limit. To facilitate understanding, the anodic portion of the cyclic voltammograms for Pt and Pt_{90}–Ir_{10} electrodes are also shown. Fig. 13a shows that in the case of Pt electrode the Qc/Qa ratio remains equal to 1 until it decreases when the upper potential limit becomes more positive than −0.4 V, which potential corresponds to the onset of the ammonia oxidation peak. This indicates that the dehydrogenation/hydrogenation of ammonia is reversible (Qc = Qa) for potential more negative than −0.4 V and also, that NH_3 can be oxidized in NH_x species at −0.62 V. However, these intermediates can be reduced back to ammonia during the reverse scan. When the positive potential limit is increased, the progressive decrease of the Qc/Qa ratio indicates that the electrode becomes covered by intermediates more

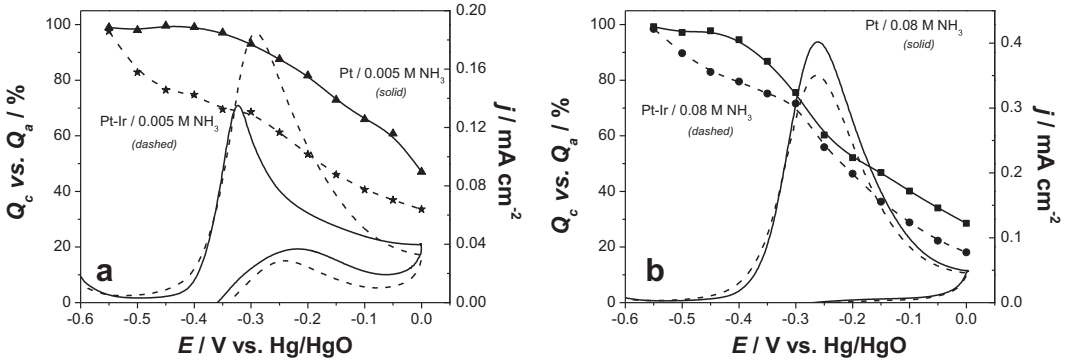

Fig. 13. Anodic charge/cathodic charge ratio for the NH_x/NH_3 reversible redox reaction (at −0.62 V) as a function of the reversal potential for [NH_3] = 0.005 M and 0.08 M). Cyclic voltammograms of electrodeposited Pt (solid line) and Pt_{90}–Ir_{10} (dashed line) for two ammonia concentrations: a) 0.005 M NH_3 and b) 0.08 M NH_3. Supporting electrolyte 1 M KOH. Scan rate = 20 mV s^{-1}.

strongly adsorbed and perhaps more dehydrogenated. The presence of these species could explain the cathodic current observed in Fig. 12 from −0.4 to −0.8 V. Interestingly for the $Pt_{90}Ir_{10}$ electrode, the Qc/Qa ratio (Fig. 13a) decreases when the upper potential limit is set between −0.55 and −0.4 V. At such negative potentials, the presence of N_{ads} species at the electrode surface is unlikely [17,21], indicating that NH_3 is oxidized into intermediates ($NH_{x,ads}$) but the fact that the cathodic charge of the peak at −0.62 V is smaller than the anodic charge leads to the conclusion that on a Pt_{90}–Ir_{10} electrode, the reaction intermediates are able to recombine and to be further oxidized, most likely to nitrogen [13]. This would explain the higher anodic currents recorded for a Pt_{90}–Ir_{10} electrode in comparison to a Pt electrode between −0.55 and −0.4 V. When the positive potential limit is set at potential more positive for the Pt_{90}–Ir_{10} electrode, a similar trend than on Pt is observed as the Qc/Qa ratio decreases, probably due to an electrode poisoning.

The electrochemical behavior of Pt and $Pt_{90}Ir_{10}$ electrodes in the presence of a higher ammonia concentration (0.08 M) is presented in Fig. 13b. For the Pt electrode, NH_3 is dehydrogenated at −0.62 V and when the potential reaches −0.40 V ammonia is oxidized to nitrogen. The drop of the Qc/Qa ratio value is attributed to the recombination of NH_x species and their subsequent irreversible oxidation to N_2 (and thus the intermediates cannot be reduced back to ammonia during the reverse scan) [21]. From −0.25 to 0 V, the increase of the slope of the plot suggests that the oxidation involves new reaction intermediates. Indeed, the potential at which the slope changes corresponds to the potential of the NH_3 oxidation peak. This rapid drop of current after the peak corresponds to Pt electrode deactivation [17]. This would indicates that for potential more positive than −0.25 V, N_{ads} can be formed and poisons the Pt surface. The behavior of the Pt_{90}–Ir_{10} electrode is interesting because, like for a lower concentration of ammonia, the Qc/Qa ratio diminishes early reinforcing the hypothesis that NH_3 and its oxidized adsorbates ($NH_{x,ads}$) are more weakly adsorbed on Ir than on Pt [17] and that a lower coverage is required to permit recombination of two molecules and their subsequent oxidation in N_2.

From the above observations, it can be concluded that Ir permits to lower the adsorption energy of $NH_{x,ads}$ moieties and thus that recombination of two intermediates is favored when Ir is alloyed to Pt. Unfortunately, Ir does not provide good electrocatalytic activity toward NH_3 oxidation and therefore its benefit can be only observed when ammonia concentration is lower than 0.02 M or when the potential is close to the onset of the NH_3 oxidation peak (between −0.55 and −0.4 V) [17,29].

The two major aims of this work were to investigate the influence of deposition parameters on the atomic composition of the $Pt_{(x)}$–$Ir_{(1-x)}$ electrodes and the activity of the resulting bimetallic electrodes for the electrochemical oxidation of ammonia. In this study, the coelectrodeposition on carbon electrode of Pt–Ir deposits having various atomic ratios was successfully achieved. This report differs from recently published works which investigated a smaller range of Pt–Ir ratios for deposits prepared by electrodeposition [28] or Pt–Ir nanoparticles obtained by chemical methods and subsequently casted on a metallic substrate [7]. Our results indicate that the faradaic efficiency for Ir deposition is lower than that of Pt because the resulting deposit is always richer in Pt than Ir when compared to the composition of the metal complexes in the deposition solution. Our work builds on previous published reports on $Pt_{(x)}$–$Ir_{(1-x)}$ electrodes [7,8,12,24–29] and describes a thorough study of the effect of electrode composition, ammonia concentration and range of potential scanning in the presence of ammonia on the activity the electrodes for the electrochemical oxidation of ammonia. Pure platinum electrode shows, in most cases, the highest activity and only in very specific and restricted conditions do $Pt_{(x)}$–$Ir_{(1-x)}$ electrodes display better activity.

4. Conclusion

$Pt_{(x)}$–$Ir_{(1-x)}$ electrodes were successfully electrodeposited onto graphite and glassy carbon substrates. By varying the deposition conditions, electrodes with Ir content varying from less than 5 to 55 at. % can be obtained. The bulk and the surface of the catalysts were found to be almost similar. Electrochemical study of these catalysts in the presence of ammonia allows to conclude that the activity for NH_3 oxidation depends on the electrode composition. An increase of the amount of iridium leads to a decrease of the activity of the $Pt_{(x)}$–$Ir_{(1-x)}$ electrodes. Interestingly, for ammonia concentrations lower than 0.02 M, the Pt_{90}–Ir_{10} electrodes show better electrocatalytic activity than pure Pt. In all cases, Ir permits to shift the onset of the NH_3 oxidation towards more negative potential and lower the poisoning effect. For low oxidation potential (from −0.55 to −0.4 V), the $Pt_{90}Ir_{10}$ electrode displays higher activity because NH_x molecules are weakly adsorbed in comparison to pure Pt due to the presence of Ir. This enhances the capacity of the NH_x intermediates to recombine and thus to be further oxidized into N_2. In this work, we demonstrated that only Pt-rich (Pt at. % > 85–90) Pt–Ir binary electrodes could be considered as better catalysts than Pt but only for some specific applications such as oxidation of NH_3 at low potential (less negative than −0.4 V) and/or for low ammonia concentration (<0.02 M).

Acknowledgements

The authors would like to thank the Natural Sciences and Engineering Research Council of Canada (NSERC) for financial support of this work, D. Karpuzov (University of Alberta, Edmonton) for XPS measurements, C. Chabanier (Institut National de la Recherche Scientifique, Varennes) for XRD analyses and P. Plamondon (Université de Montréal, Montréal) for SEM observations.

References

[1] K.W. Kim, Y.J. Kim, I.T. Kim, G.I. Park, E.H. Lee, Electrochimica Acta 50 (2005) 4356–4364.
[2] K.W. Kim, Y.J. Kim, I.T. Kim, G.I. Park, E.H. Lee, Water Research 40 (2006) 1431–1441.
[3] A. Kapalka, S. Fierro, Z. Frontistis, A. Katsaounis, O. Frey, M. Koudelka, C. Comninellis, K.M. Udert, Electrochemistry Communications 11 (2009) 1590–1592.
[4] A. Kapałka, L. Joss, Á. Anglada, C. Comninellis, K.M. Udert, Electrochemistry Communications 12 (2010) 1714–1717.
[5] D. Reyter, D. Bélanger, L. Roué, Water Research 44 (2010) 1918–1926.
[6] D. Reyter, D. Bélanger, L. Roué, Journal of Hazardous Materials 192 (2011) 507–513.
[7] F.J. Vidal-Iglesias, J. Solla-Gullón, V. Montiel, J.M. Feliu, A. Aldaz, Journal of Power Sources 171 (2007) 448–456.
[8] F. Vitse, M. Cooper, G.G. Botte, Journal of Power Sources 142 (2005) 18–26.
[9] M. Cooper, G.G. Botte, Journal of the Electrochemical Society 153 (2006) A1894–A1901.
[10] A. Klerke, C.H. Christensen, J.K. Norskov, T. Vegge, Journal of Materials Chemistry 18 (2008) 2304–2310.
[11] B.K. Boggs, G.G. Botte, Journal of Power Sources 192 (2009) 573–581.
[12] M. Muthuvel, G.G. Botte, in: R.E. White (Ed.), Modern Aspects of Electrochemistry, Springer, New York, 2009, pp. 207–243.
[13] V. Rosca, M. Duca, M.T. DeGroot, M.T.M. Koper, Chemical Reviews 109 (2009) 2209–2244.
[14] N.J. Bunce, D. Bejan, Electrochimica Acta 56 (2011) 8085–8093.
[15] H. Gerischer, A. Mauerer, Journal of Electroanalytical Chemistry 25 (1970) 421–433.
[16] S. Wasmus, E.J. Vasini, M. Krausa, H.T. Mishima, W. Vielstich, Electrochimica Acta 39 (1994) 23–31.
[17] A.C.A. De Vooys, M.T.M. Koper, R.A. Van Santen, J.A.R. Van Veen, Journal of Electroanalytical Chemistry 506 (2001) 127–137.
[18] F.J. Vidal-Iglesias, N. Garcia-Araez, V. Montiel, J.M. Feliu, A. Aldaz, Electrochemistry Communications 5 (2003) 22–26.
[19] F.J. Vidal-Iglesias, J. Solla-Gullon, P. Rodriguez, E. Herrero, V. Montiel, J.M. Feliu, A. Aldaz, Electrochemistry Communications 6 (2004) 1080–1084.
[20] F.J. Vidal-Iglesias, J. Solla-Gullon, V. Montiel, J.M. Feliu, A. Aldaz, Journal of Physical Chemistry B 109 (2005) 12914–12919.

[21] V. Rosca, M.T.M. Koper, Physical Chemistry Chemical Physics 8 (2006) 2513–2524.
[22] F.J. Vidal-Iglesias, J. Solla-Gullon, J.M. Feliu, H. Baltruschat, A. Aldaz, Journal of Electroanalytical Chemistry 588 (2006) 331–338.
[23] L. Candido, J.A.C.P. Gomes, Materials Chemistry and Physics 129 (2011) 1146–1151.
[24] B.A. Lopez De Mishima, D. Lescano, T. Molina Holgado, H.T. Mishima, Electrochimica Acta 43 (1998) 395–404.
[25] K. Endo, K. Nakamura, Y. Katayama, T. Miura, Electrochimica Acta 49 (2004) 2503–2509.
[26] E.P. Bonnin, E.J. Biddinger, G.G. Botte, Journal of Power Sources 182 (2008) 284–290.
[27] E. Moran, C. Cattaneo, H. Mishima, B.A. Lopez De Mishima, S.P. Silvetti, J.L. Rodriguez, E. Pastor, Journal of Solid State Electrochemistry 12 (2008) 583–589.
[28] B.K. Boggs, G.G. Botte, Electrochimica Acta 55 (2010) 5287–5293.
[29] T.L. Lomocso, E.A. Baranova, Electrochimica Acta 56 (2011) 8551–8558.
[30] C. Paoletti, A. Cemmi, L. Giorgi, R. Giorgi, L. Pilloni, E. Serra, M. Pasquali, Journal of Power Sources 183 (2008) 84–91.
[31] L. Vázquez-Gómez, S. Cattarin, R. Gerbasi, P. Guerriero, M. Musiani, Journal of Applied Electrochemistry 39 (2009) 2165–2172.
[32] J.V. Zoval, J. Lee, S. Gorer, R.M. Penner, Journal of Physical Chemistry B 102 (1998) 1166–1175.
[33] F. Gloaguen, J.M. Léger, C. Lamy, A. Marmann, U. Stimming, R. Vogel, Electrochimica Acta 44 (1999) 1805–1816.
[34] V.I. Kravtsov, Russian Journal of Electrochemistry 36 (2000) 1209–1215.
[35] M.M.E. Duarte, A.S. Pilla, J.M. Sieben, C.E. Mayer, Electrochemistry Communications 8 (2006) 159–164.
[36] E.L. MacNamara, Journal of the Electrochemical Society 109 (1962) 61–63.
[37] T. Ohsaka, M. Isaka, K. Hirano, T. Ohishi, Ultrasonics Sonochemistry 15 (2008) 283–288.
[38] E.N. El Sawy, V.I. Birss, Journal of Materials Chemistry 19 (2009) 8244–8252.
[39] A.G. Munoz, H.J. Lewerenz, Journal of the Electrochemical Society 156 (2009) 184–187.
[40] S. Le Vot, L. Roué, D. Bélanger, Electrochimica Acta 59 (2012) 49–56.
[41] F. Béguin, M. Friebe, K. Jurewicz, C. Vix-Guterl, J. Dentzer, E. Frackowiak, Carbon 44 (2006) 2392–2398.
[42] J. Greeley, T.F. Jaramillo, J. Bonde, I. Chorkendorff, J.K. Norskov, Nature Materials 5 (2006) 909–913.
[43] J. Solla-Gullon, P. Rodriguez, E. Herrero, A. Aldaz, J.M. Feliu, Physical Chemistry Chemical Physics 10 (2008) 1359–1373.
[44] J.M. Dona Rodriguez, J.A.H. Melian, J.P. Pena, Journal of Chemical Education 77 (2000) 1195–1197.
[45] T. Pajkossy, L.A. Kibler, D.M. Kolb, Journal of Electroanalytical Chemistry 600 (2007) 113–118.
[46] S. Trasatti, O.A. Petrii, Journal of Electroanalytical Chemistry 327 (1992) 353–376.
[47] A.J. Motheo, S.A.S. Machado, M.H. Van Kampen, J.R. Santos Jr., Journal of Brazilian Chemical Society 4 (1993) 122–127.
[48] A.N. Correia, L.H. Mascaro, S.A.S. Machado, L.A. Avaca, Electrochimica Acta 42 (1997) 493–495.
[49] L. Vázquez-Gómez, S. Cattarin, P. Guerriero, M. Musiani, Electrochimica Acta 53 (2008) 8310–8318.
[50] J.L. Zubimendi, L. Vazquez, P. Ocon, J.M. Vara, W.E. Triaca, R.C. Salvarezza, A.J. Arvia, Journal of Physical Chemistry 97 (1993) 5095–5102.
[51] J. Heinze, A. Rasche, M. Pagels, B. Geschke, Journal of Physical Chemistry B 111 (2007) 989–997.
[52] E.N. El Sawy, V.I. Birss, in: 217th ECS Meeting, Vancouver, BC, 2010, pp. 195–201.
[53] A. Petrossians, J.J. Whalen Iii, J.D. Weiland, F. Mansfeld, Journal of the Electrochemical Society 158 (2011) D269–D276.
[54] S. Le Vot, D. Reyter, L. Roue, D. Belanger, Journal of the Electrochemical Society 159 (2012) F91–F96.
[55] T. Ioroi, K. Yasuda, Journal of the Electrochemical Society 152 (2005) 1917–1924.
[56] J. Wang, P. Holt-Hindle, D. MacDonald, D.F. Thomas, A. Chen, Electrochimica Acta 53 (2008) 6944–6952.
[57] J. Augustynski, M. Koudelk, J. Sanchez, B.E. Conway, Journal of Electroanalytical Chemistry 160 (1984) 233–248.
[58] Z. Liu, J.Y. Lee, W. Chen, M. Han, L.M. Gan, Langmuir 20 (2004) 181–187.
[59] Y. Liang, H. Zhang, H. Zhong, X. Zhu, Z. Tian, D. Xu, B. Yi, Journal of Catalysis 238 (2006) 468–476.
[60] S. Hu, L. Xiong, X. Ren, C. Wang, Y. Luo, International Journal of Hydrogen Energy 34 (2009) 8723–8732.
[61] B.D. El-Issa, A. Katrib, R. Ghodsian, B.A. Salsa, S.H. Addassi, International Journal of Quantum Chemistry 33 (1988) 195–216.
[62] F. Wu, H. Murakami, Y. Yamabe-Mitarai, H. Harada, H. Katayama, Y. Yamamoto, Surface and Coatings Technology 184 (2004) 24–30.
[63] M.T.M. Koper, Nanoscale 3 (2011) 2054–2073.